JACS
JOURNAL OF THE AMERICAN CHEMICAL SOCIETY

Communication

pubs.acs.org/JACS

Surface-Alkalinization-Induced Enhancement of Photocatalytic H_2 Evolution over $SrTiO_3$-Based Photocatalysts

Shuxin Ouyang,[†] Hua Tong,[‡,§] Naoto Umezawa,[†,§,∥] Junyu Cao,[†] Peng Li,[†,‡] Yingpu Bi,[‡] Yuanjian Zhang,[‡] and Jinhua Ye*[,†,‡,§]

[†]Environmental Remediation Materials Unit, National Institute for Materials Science (NIMS), 1-2-1 Sengen, Tsukuba, Ibaraki 305-0047, Japan

[‡]International Center for Materials Nanoarchitectonics (WPI-MANA), National Institute for Materials Science (NIMS), 1-2-1 Sengen, Tsukuba, Ibaraki 305-0047, Japan

[§]TU−NIMS Joint Research Center, School of Materials Science and Engineering, Tianjin University, 92 Weijin Road, Nankai District, Tianjin 300072, P. R. China

[∥]PRESTO, Japan Science and Technology Agency (JST), 4-1-8 Honcho, Kawaguchi, Saitama 332-0012, Japan

Supporting Information

ABSTRACT: A strategy of reaction-environment modulation was employed to change the surface property of a semiconductor photocatalyst to enhance its photocatalytic performance. Surface alkalinization induced by a high alkalinity of the solution environment significantly shifted the surface energy band of a $SrTiO_3$ photocatalyst to a more negative level, supplying a strong potential for H_2O reduction and consequently promoting the photocatalytic efficiency of H_2 evolution. This mechanism is also applicable for visible-light-sensitive La,Cr-codoped $SrTiO_3$ photocatalyst, which hence, could achieve a high apparent quantum efficiency of 25.6% for H_2 evolution in CH_3OH aqueous solution containing 5 M NaOH at an incident wavelength of 425 ± 12 nm.

Semiconductor photocatalysis supplies an environmentally friendly approach for splitting water to produce clean hydrogen energy and completely decomposing organic contaminants with the assistance of solar light, and thus, it is considered to be a potential solution for counteracting the energy shortage and realizing environmental remediation.[1−3] However, the relatively low photocatalytic efficiency is still one of the most important factors restricting the practical application of this technology. Various strategies have been developed to enhance the photocatalytic performance. For example, energy-band engineering effectively extends the light absorption of the photocatalyst into the visible region and meanwhile manipulates the levels of the band edges to offer adequate redox potentials.[4−8] Morphology tailoring of the photocatalyst can increase the surface area to generate more active sites,[9−11] expose high-surface-energy facets to promote adsorption and reaction activity,[12−14] or construct special microstructures to localize the incident light.[15] Loaded novel cocatalysts enhance the separation of photocarriers in the surface to supply facile channels for redox reactions,[4,16,17] or serve as visible-light sensitizers to inject more photocarriers for photocatalytic reactions.[18,19] It is obvious that the current strategies are mainly focused on the photocatalyst itself, but the reaction environment is usually ignored.

Photocatalytic reaction is also a surface-contact reactive process, just as traditional catalysis. The reaction environment plays a significant role in the surface properties and thus affects the photocatalytic efficiency. In 1980, Wagner and Somorjai[20] reported direct photocatalytic H_2 production from a high-alkalinity aqueous solution ([NaOH] > 5 M) over a noble-metal-free $SrTiO_3$(111) single crystal. However, the surface area of the single crystal was very small, resulting in a relatively low photocatalytic efficiency even at alkalinity as high as [NaOH] = 20 M. Moreover, the detailed mechanism was not clarified, although a simple surface model was proposed to explain that this phenomenon could be attributed to the suppression of photocarrier recombination. Herein we demonstrate a strategy of reaction-environment modulation to change the surface properties of $SrTiO_3$-based nanocrystal photocatalysts, which induces an advantageous shift of the surface energy band and hence significantly promotes the photocatalytic efficiency of H_2 evolution.

Nanocrystals of $SrTiO_3$ (STO) and La,Cr-codoped $SrTiO_3$ (La,Cr-STO) were synthesized using a typical sol−gel hydrothermal process (for details, see section SI-1 in the Supporting Information). Figure 1a shows the powder X-ray diffraction (PXRD) patterns of the as-prepared samples, which reveal that both the pure and doped materials possess a homogeneous crystal structure of cubic perovskite symmetry. Since the La and Cr substitute the Sr and Ti, respectively, and the radius of La (1.032 Å) is smaller than that of Sr (1.180 Å) while the radius of Cr (0.615 Å) is bigger than that of Ti (0.605 Å), the peak positions of the La,Cr-STO sample are almost the same as those of STO. Figure 1b shows the UV−vis absorption spectra of STO and La,Cr-STO. After doping, the Cr 3d levels are inserted into the original band gap of STO, which induces an obvious absorption in the visible region. The Cr doping has been shown to be a feasible approach for extending the light absorption of STO into the visible region, but only Cr with +3

Received: November 11, 2011
Published: January 12, 2012

dx.doi.org/10.1021/ja210610h | J. Am. Chem.Soc. 2012, 134, 1974−1977

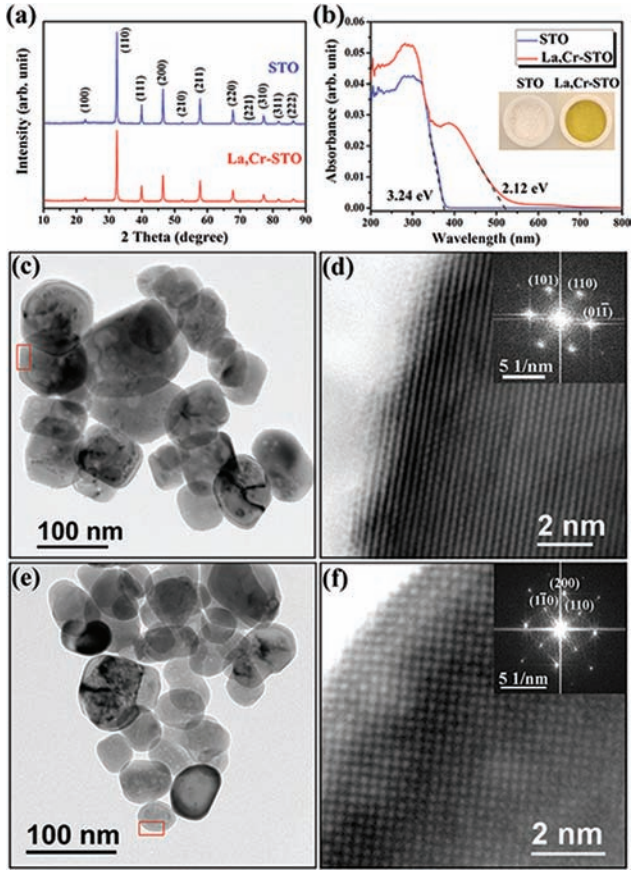

Figure 1. (a) PXRD patterns and (b) UV−vis absorption spectra of STO and La,Cr-STO samples. (c) TEM and (d) HRTEM [selected region in (c)] images of the STO sample. (e) TEM and (f) HRTEM [selected region in (e)] images of the La,Cr-STO sample. The insets in (d) and (f) are SAED patterns.

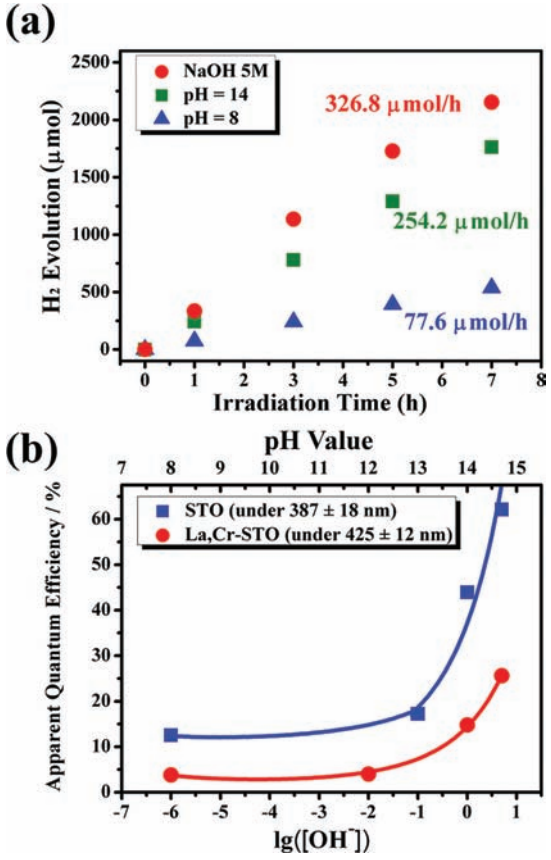

Figure 2. (a) H_2 evolution over the La,Cr-STO sample under visible-light irradiation (λ > 400 nm). (b) Apparent quantum efficiencies of H_2 evolution over STO and La,Cr-STO at various pH values. (Light intensity: 387 ± 18 nm, 0.85 mW/cm^2; 425 ± 12 nm, 1.0 mW/cm^2.)

chemical valence is beneficial for H_2 evolution.[21,22] In this study, A-site La doping in STO was used to suppress the appearance of Cr^{6+} in the B sites. The energy-dispersive X-ray (EDX) spectra of a typical single particle showed that La and Cr were doped into STO successfully (section SI-2). Figure 1c−f display the typical transmission electron microscopy (TEM) and high-resolution TEM (HRTEM) images of STO and La,Cr-STO samples. It can be clearly observed that all of these samples are monodispersed as irregular particles with the average diameters of 80 nm for STO [Brunauer−Emmett−Teller (BET) surface area 11.4 m^2/g] and 60 nm for La,Cr-STO (BET surface area 16.6 m^2/g). The homogeneous lattice patterns in the HRTEM images and the regular crystal diffraction spots in the selected-area electron diffraction (SAED) patterns (Figure 1d,f) reveal the single-crystalline nature of each particle for both the STO and La,Cr-STO samples.

Photocatalytic H_2 evolution was carried out with the STO or La,Cr-STO photocatalyst (loaded 0.5 wt % Pt cocatalyst) suspended in a CH_3OH solution. Figure 2a depicts the H_2 evolution over the La,Cr-STO sample under visible-light irradiation. When the as-prepared La,Cr-STO sample was naturally suspended in CH_3OH solution, the pH value of the solution slightly increased to ∼8 because of the desorption of OH^- from the sample surface. Under such conditions, the rate of H_2 evolution was 77.6 μmol/h, which is comparable to that reported for Sb,Cr-codoped STO (Sb and Cr codoping in the B sites).[21] However, when the pH value was adjusted to 14, a more than 2-fold enhancement of the H_2 evolution rate was observed. Further increasing the concentration of NaOH up to 5 M increased the H_2 evolution rate to 326.8 μmol/h. It is obvious that increasing alkalinity can promote the photocatalytic performance of H_2 evolution over the La,Cr-STO sample. Measurements of the alkalinity-dependent apparent quantum efficiency were employed to confirm the universal phenomenon over STO-based photocatalysts. As plotted in Figure 2b, the apparent quantum efficiencies of UV-irradiated STO and visible-light-irradiated La,Cr-STO are strongly dependent on the alkalinity of the CH_3OH solution. Interestingly, for both the STO and La,Cr-STO samples, the H_2 evolution rate increased slightly when the pH value was lower than 13 but was significantly enhanced at pH >13. It is noteworthy that the La,Cr-STO sample achieved a high apparent quantum efficiency of 25.6% for H_2 evolution in CH_3OH aqueous solution containing 5 M NaOH at an incident wavelength of 425 ± 12 nm, which is obviously higher than those of most of the reported oxide photocatalysts.[2,22−24]

STO thin films were prepared to investigate the variation tendency of the alkalinity-dependent photocatalytic activity of H_2 evolution via photoelectrochemical and photoinduced hydrophilic characterizations. First, photoelectrochemical measurements were used to determine the approximate band-edge potentials. As illustrated in Figure 3a, in the absence of a bias potential, an obvious photocurrent over the STO thin film was observed, and the current intensity exhibited a trend consistent

dx.doi.org/10.1021/ja210610h | J. Am. Chem.Soc. 2012, 134, 1974−1977

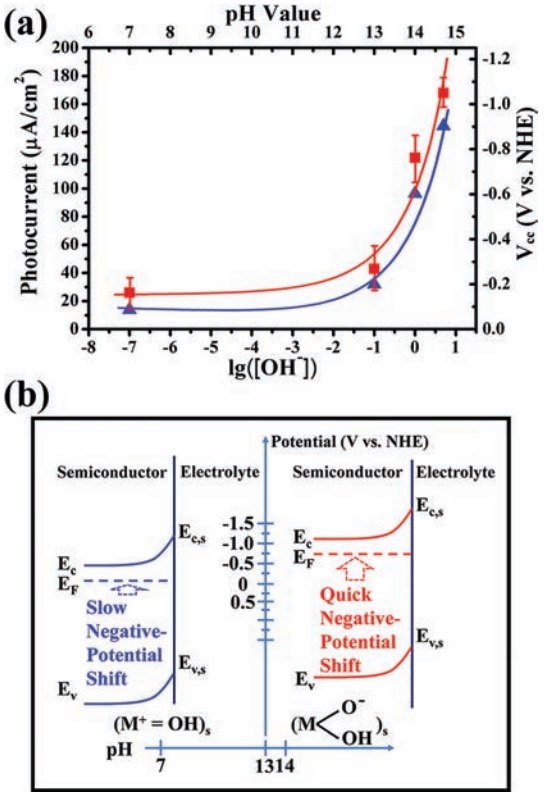

Figure 3. (a) Photoelectrochemical properties (photocurrent and closed-circuit potential V_{cc}) of an STO thin film at various pH values. (b) Schematic mechanism of the effect of alkalinity on the electrode potential.

with that of the photocatalytic activity, confirming that photoelectrochemical tests could be employed to figure out the variation of the alkalinity-dependent photocatalytic activity of H_2 evolution. We also measured the closed-circuit potential (V_{cc}) over the STO thin film (for details see section SI-1.4). Actually, this potential showed a negative shift with increasing alkalinity and was also consistent with the alteration tendencies of the photocurrent and photocatalytic efficiency. However, the intrinsic reason for this phenomenon still needs to be explored.

As we know, the surface properties of oxide semiconductors are significantly influenced by the solution environment and exhibit two typical kind of surfaces, as shown in eqs 1 and 2:[25]

$$(M=O)_s + H_2O \rightleftharpoons (M^+=OH)_s + OH^- \quad (1)$$

$$(M=O)_s + H_2O \rightleftharpoons (M\langle^{O^-}_{OH})_s + H^+ \quad (2)$$

As the alkalinity increases, the oxide surface is converted from positively charged (eq 1) to negatively charged (eq 2), as shown in Figure 3b. For these surface-balanced reactions, according to the Nernst equation, the redox potential shift $\Delta\phi$ can be calculated as follows:

$$\Delta\phi = -2.3\left(\frac{kT}{e}\right)\alpha \times \mathrm{pH} \quad (3)$$

in which k, T, and e signify the Boltzmann constant, system temperature, and elementary charge, respectively. In this equation, the parameter α indicates the extent to which the balanced reaction proceeds. For larger values of α, the balanced reaction will be more right-shifted, and thus, the surface will generate more hydroxyl radicals (eq 2). It is well-known that the hydroxyl radical is a typical nonionic surfactant that greatly affects the surface hydrophilic properties, and thus, contact angle measurements indirectly reflect the concentration of hydroxyl radical on the surface.[26,27] Figure 4 depicts the variation of the contact angle with increasing alkalinity of the reaction solution, and the insets show images of water drops on an STO thin film at various pH values. It can be observed that the variation tendency of the contact angle versus alkalinity is similar to an exponential correlation. Since the concentration of hydroxyl radical depends almost linearly on the contact angle,[27] it can be deduced that the concentration of hydroxyl radical versus the alkalinity is close to an exponential trend, which means that α changes nearly exponentially with increasing alkalinity. Therefore, in eq 3, while k, T, and e are constants and the pH changes linearly, α shows a nearly exponential alteration. Thus, it is easy to understand that the potentials of the band edges of STO shift according to an exponential-variation trend with increasing alkalinity of the reaction solution. This exponential variation of the band-edge shift can get ahead of the linear shift of the H_2 production potential versus pH on the metal electrode or cocatalyst, contributing to the enhancement of the photocatalytic efficiency.

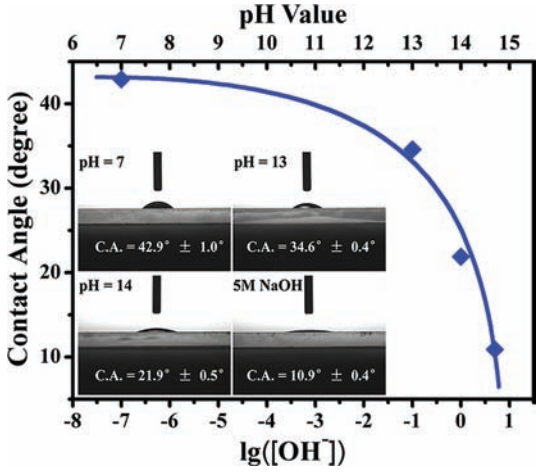

Figure 4. Effect of alkalinity on the photoinduced hydrophilic properties over STO thin films as determined by contact angle measurements.

Surface electronic structure calculations based on the density functional theory (DFT) + U approach[28] were also carried out to study the band-edge shift of STO (see section SI-1.6). Models of the $SrTiO_3$(110) surface with and without OH^- adsorption were used for the comparison of the density of states. It is clearly shown that both the valence and conduction band edges are higher in the model with OH^- adsorption than in the absence of OH^-, which is consistent with the experimental observations (see section SI-3).

Figure 3b summarizes the schematic mechanism of the effect of alkalinity on the electrode potential. With an increase in the pH value, the positively charged surface is transformed to a negatively charged one. The concentration of adsorbed hydroxide ions on the surface determines the extent of the band-edge shift of the STO sample. When the pH value is less than 13, the negative shifts of the band edge of the surface energy band are limited. However, when the pH value is greater than 13, a large number of hydroxide ions are adsorbed on the

dx.doi.org/10.1021/ja210610h | J. Am. Chem.Soc. 2012, 134, 1974–1977

STO surface, which induces the significantly negative shift of the band edge of the surface conduction band ($E_{c,s}$) to enhance the reductive potential. Although the band edge of the surface valence band ($E_{v,s}$) also migrates to a more negative level to suppress the oxidative capability, the large amount of adsorbed hydroxide ions are beneficial to combine with holes effectively to generate hydroxyl radicals and then oxidize CH_3OH quickly, which facilitates the separation of photocarriers in the surface (see section SI-4).[20] Because of the above-mentioned favorable factors, the photocatalytic efficiency of H_2 evolution over the STO photocatalyst is greatly promoted. Since this phenomenon is induced by the surface property affecting the intrinsic surface band structure, this mechanism is also available for La,Cr-STO sample, which therefore can achieve high photocatalytic activity for H_2 evolution under visible-light irradiation.

In summary, we have demonstrated that surface alkalinization can induce a negative shift of the band edge of the surface conduction band in STO-based oxide photocatalysts, especially above pH 13. The strong reduction potential caused by the high alkalinity of the reaction environment can significantly enhance the photocatalytic performance of H_2 evolution. For example, the La,Cr-STO photocatalyst achieved a high apparent quantum efficiency of 25.6% for H_2 evolution in CH_3OH aqueous solution containing 5 M NaOH at an incident wavelength of 425 ± 12 nm. This strategy of surface alkalinization will probably be applicable for other oxide semiconductors that are stable in highly alkaline solutions and thus may supply a novel and facile approach for promoting their photocatalytic activity of H_2 evolution, photoelectric conversion efficiency, and CO_2 photoreduction performance.

■ ASSOCIATED CONTENT

Supporting Information

Experimental and calculational procedures, TEM and EDX measurements for La,Cr-STO, calculations on surface electronic structures of $SrTiO_3$, and schematic illustration of alkalinity-induced separation of carriers. This material is available free of charge via the Internet at http://pubs.acs.org.

■ AUTHOR INFORMATION

Corresponding Author

jinhua.ye@nims.go.jp

Notes

The authors declare no competing financial interest.

■ ACKNOWLEDGMENTS

This work was partially supported by the World Premier International Research Center Initiative on Materials Nanoarchitectonics, MEXT; the Global COE Program of the Tokyo Institute of Technology; and the Japan Science and Technology Agency (JST) Precursory Research for Embryonic Science and Technology (PRESTO) Program.

■ REFERENCES

(1) Hoffmann, M. R.; Martin, S. T.; Choi, W. Y.; Bahnemann, D. W. *Chem. Rev.* **1995**, *95*, 69.
(2) Chen, X. B.; Shen, S. H.; Guo, L. J.; Mao, S. S. *Chem. Rev.* **2010**, *110*, 6503.
(3) Tong, H.; Ouyang, S. X.; Bi, Y. P.; Umezawa, N.; Oshikiri, M.; Ye, J. H. *Adv. Mater.* **2012**, *24*, 229.
(4) Maeda, K.; Teramura, K.; Lu, D. L.; Takata, T.; Saito, N.; Inoue, Y.; Domen, K. *Nature* **2006**, *440*, 295.
(5) Wang, D. F.; Kako, T.; Ye, J. H. *J. Am. Chem. Soc.* **2008**, *130*, 2724.
(6) Ouyang, S. X.; Kikugawa, N.; Chen, D.; Zou, Z. G.; Ye, J. H. *J. Phys. Chem. C* **2009**, *113*, 1560.
(7) Yu, H. G.; Irie, H.; Hashimoto, K. *J. Am. Chem. Soc.* **2010**, *132*, 6898.
(8) Ouyang, S. X.; Ye, J. H. *J. Am. Chem. Soc.* **2011**, *133*, 7757.
(9) Huang, J. H.; Ma, R.; Ebina, Y.; Fukuda, K.; Takada, K.; Sasaki, T. *Chem. Mater.* **2010**, *22*, 2582.
(10) Fan, X. X.; Wang, Y.; Chen, X. Y.; Gao, L.; Luo, W. J.; Yuan, Y. P.; Li, Z. S.; Yu, T.; Zhu, J. H.; Zou, Z. G. *Chem. Mater.* **2010**, *22*, 1276.
(11) Yan, S. C.; Ouyang, S. X.; Gao, J.; Yang, M.; Feng, J. Y.; Fan, X. X.; Wan, L. J.; Li, Z. S.; Ye, J. H.; Zhou, Y.; Zou, Z. G. *Angew. Chem., Int. Ed.* **2010**, *49*, 6400.
(12) Liu, S. W.; Yu, J. G.; Jaroniec, M. *J. Am. Chem. Soc.* **2010**, *132*, 11914.
(13) Ahmed, A. Y.; Kandiel, T. A.; Oekermann, T.; Bahnemann, D. *J. Phys. Chem. Lett.* **2011**, *2*, 2461.
(14) Bi, Y. P.; Ouyang, S. X.; Umezawa, N.; Cao, J. Y.; Ye, J. H. *J. Am. Chem. Soc.* **2011**, *133*, 6490.
(15) Li, H. X.; Bian, Z. F.; Zhu, J.; Zhang, D. Q.; Li, G. S.; Huo, Y. N.; Li, H.; Lu, Y. F. *J. Am. Chem. Soc.* **2007**, *129*, 8406.
(16) Yan, H. J.; Yang, J. H.; Ma, G. J.; Wu, G. P.; Zong, X.; Lei, Z. B.; Shi, J. Y.; Li, C. *J. Catal.* **2009**, *266*, 165.
(17) Wang, D. F.; Pierre, A.; Kibria, M. G.; Cui, K.; Han, X. G.; Bevan, K. H.; Guo, H.; Paradis, S.; Hakima, A. R.; Mi, Z. T. *Nano Lett.* **2011**, *11*, 2353.
(18) Hensel, J.; Wang, G. M.; Li, Y.; Zhang, J. Z. *Nano Lett.* **2010**, *10*, 478.
(19) Wang, G. M.; Yang, X. Y.; Qian, F.; Zhang, J. Z.; Li, Y. *Nano Lett.* **2010**, *10*, 1088.
(20) Wagner, F. T.; Somorjai, G. A. *Nature* **1980**, *285*, 559.
(21) Kato, H.; Kudo, A. *J. Phys. Chem. B* **2002**, *106*, 5029.
(22) Wang, D. F.; Ye, J. H.; Kako, T.; Kimura, T. *J. Phys. Chem. B* **2006**, *110*, 15824.
(23) Konta, R.; Ishii, T.; Kato, H.; Kudo, A. *J. Phys. Chem. B* **2004**, *108*, 8992.
(24) Kim, H. G.; Borse, P. H.; Jang, J. S.; Jeong, E. D.; Jung, O. S.; Suh, Y. J.; Lee, J. S. *Chem. Commun.* **2009**, 5889.
(25) Gurevich, Y. Y.; Pleskov, Y. V.; Rotenberg, Z. A. *Photoelectrochemistry*; Consultants Bureau: New York, 1980.
(26) Sakai, N.; Wang, R.; Fujishima, A.; Watanabe, T.; Hashimoto, K. *Langmuir* **1998**, *14*, 5918.
(27) Sakai, N.; Fujishima, A.; Watanabe, T.; Hashimoto, K. *J. Phys. Chem. B* **2003**, *107*, 1028.
(28) Anisimov, V. I.; Zaanen, J.; Andersen, O. K. *Phys. Rev. B* **1991**, *44*, 943.